Monocarboxylate transporter antagonism reveals metabolic vulnerabilities of viral-driven lymphomas

Emmanuela N. Bonglack[1,2], Joshua E. Messinger[2], Jana M. Cable[2], K. Mark Parnell[3], James Ch'ng[4], Heather R. Christofk[5], and Micah A. Luftig[2#].

[1]Department of Pharmacology and Cancer Biology, Duke University School of Medicine, Durham, NC, 27710

[2]Department of Molecular Genetics and Microbiology, Duke Center for Virology, Duke University School of Medicine, Durham, NC, 27710

[3]Vettore, LLC, San Francisco, CA, 94158

[4]Department of Pediatrics, Division of Hematology/Oncology, David Geffen School of Medicine at UCLA, Los Angeles, CA, 90095

[5]Department of Biological Chemistry, David Geffen School of Medicine at UCLA, Los Angeles, CA, 90095

#Corresponding author: Micah A. Luftig

Micah.luftig@duke.edu

Phone: 919-668-3091

ABSTRACT

Epstein-Barr Virus (EBV) is a ubiquitous herpesvirus that typically causes asymptomatic infection but can promote B lymphoid tumors in the immune-suppressed. *In vitro,* EBV infection of primary B cells stimulates glycolysis during immortalization into lymphoblastoid cell lines (LCLs). Lactate export during glycolysis is crucial for continued proliferation of many cancer cells-part of a phenomenon known as the “Warburg effect,” and is mediated by the monocarboxylate transporters 1 and 4 (MCT1 and MCT4). However, the role of MCT1/4 has yet to be studied in EBV-associated malignancies which display Warburg-like metabolism *in vitro*. Here, we show that EBV infection of B lymphocytes directly promotes temporal induction of MCT1 and MCT4 through the viral proteins EBNA2 and LMP1 respectively, with MCT1 being induced early after infection and MCT4 late. Remarkably, singular MCT1 inhibition early, and dual MCT1/4 inhibition in LCLs using a novel MCT4-selective inhibitor led to growth arrest and lactate buildup. Metabolic profiling in LCLs revealed significatly reduced oxygen consumption rates (OCR) and NAD+/NADH ratios, contrary to prevous observations of increased OCR and unaltered NAD+/NADH ratios in MCT1/MCT4-inhibited cancer cells. Furthermore, U-^{13}C6 glucose labeling of MCT1/4-inhibited LCLs also revealed increased labeling of glutathione in the presence of elevated ROS and depleted glutathione pools, as well as increased labeling of *de novo* pyrimidine biosynthetic intermediates, suggesting broad effects on LCL metabolism. These vulnerabilities sensitized LCLs as well as EBV+, and the related gammaherpesvirus KSHV+ lymphoma cell lines to killing by metformin and phenformin, pointing at a novel therapeutic approach for viral lymphomas.

37 **INTRODUCTION**

38 Epstein-Barr Virus (EBV) is a ubiquitous human herpesvirus transmitted through saliva,
39 with more than 95% of the world being infected by adulthood. Primary EBV infection is typically
40 asymptomatic and surmounts to latency establishment in quiescent memory B cells in the
41 peripheral blood(1). However, in immunocompromised persons, EBV reactivation can cause
42 uncontrolled latent EBV-induced B-cell proliferation and frank lymphoma. Recent evidence
43 suggests that host responses such as the DNA damage response (DDR) and metabolic stress
44 play a significant cell-intrinsic role in preventing EBV-driven B-cell transformation(2, 3).

45 EBV infection of primary human peripheral blood B cells *in vitro* produces indefinitely
46 proliferating lymphoblastoid cell lines (LCLs). LCLs express the Latency III growth program, where
47 all six EBV Nuclear Antigens, or EBNAs, (EBNA-LP, 1, 2, 3A, 3B, and 3C) and two Latent
48 Membrane Proteins, or LMPs, (LMP1 and LMP2A/B) are present. This gene expression program
49 mimics that of many EBV-associated B-lymphoid cancers, making LCLs a suitable model for
50 studying mechanisms underlying tumorigenesis(4). Prior to Latency III establishment in LCLs and
51 shortly after EBV infection of B cells, a transient period of hyperproliferation, called Latency IIb, is
52 induced, where only the viral EBNAs are expressed in the absence of the LMPs(5, 6). This
53 culminates in an irreversible growth arrest in most cells caused by a persistent DNA Damage
54 Response (DDR)(7). However, a very small subset (<10%) of hyperproliferating cells evade host
55 barriers like the DDR, and transition into Latency III-expressing LCLs within weeks(2).

56 During EBV immortalization of B cells into LCLs, increased energetic demands for
57 continued proliferation drive an upregulation of glycolysis and extracellular acidification rates
58 (ECAR)(3, 8–10). While the ECAR is largely a reflection of lactate export into the extracellular
59 environment, the magnitude and role of lactate export during EBV-driven B-cell immortalization
60 remains poorly characterized. Besides being a glycolytic waste product, lactate has recently
61 emerged to play a key role in tumor development, growth, and metastasis(11, 12). Furthermore,
62 intracellular lactate buildup can have dire consequences on cell homeostasis due to acidification

63 by lactic acid, highlighting the importance of lactate export for sustained cell growth and
64 survival(13).

65 Proton-coupled lactate export is driven by the plasma membrane proteins
66 monocarboxylate transporters 1 and 4 (MCT1 and MCT4). MCT1 has a much higher affinity for
67 lactate than MCT4, making it the primary lactate transporter under normal physiological conditions
68 (14–16). MCT4, however, is typically expressed in highly glycolytic tissues, or when intracellular
69 lactate concentrations are high, such as during aerobic glycolysis(17–19). MCT1 and MCT4 have
70 the ability to transport other monocarboxylates such as pyruvate and ketone bodies like
71 acetoacetate and β-hydroxybutyrate(15, 19, 20). However, these transporters are most commonly
72 associated with their role in lactate transport across the plasma membrane, especially during
73 tumor development, growth, and metastasis(21–23). As such, MCT1 and MCT4 act as essential
74 buffers at the intersection of the intracellular and extracellular environments, sensing
75 monocarboxylate concentrations and facilitating rapid transport based on the needs of the
76 cell(24–26). Not surprisingly, MCT1 and MCT4 are commonly expressed in a wide variety of
77 tumors, exporting lactate from glycolytic cancer cells, which can later be recycled by oxidative
78 cells in the tumor microenvironment(27, 28).

79 Targeting MCT1 and MCT4-mediated lactate export has become a highly attractive
80 therapeutic strategy in recent years, as blocking lactate export can lead to cell cycle arrest, and
81 sensitize tumor cells to killing by other metabolic inhibitors(20, 22, 29, 30). MCT1 inhibitors are
82 currently in Phase I clinical trials for a number of solid tumors and lymphomas(31). While these
83 inhibitors have proven to effectively reduce tumor burden in preclinical models of MCT1-
84 overexpressing cancers, they are unfortunately ineffective in MCT1/MCT4-co-expressing cancers
85 due to the redundant role of MCT4 as a lactate exporter(32). This highlights the need for MCT4-
86 specific inhibitors, which are unfortunately not commercially available to date. Furthermore, while
87 inhibition of MCT1 and MCT4 universally leads to a buildup of intracellular lactate in tumor cells,
88 the mechanisms underlying growth arrest and cell death are not fully understood. Thus, studying

89 how MCT1 and MCT4 are regulated in diverse contexts is critical for expanding our understanding
90 of their role not only in tumorigenesis, but cell biology and homeostasis at large.

91 Given their established roles in tumor development both *in vitro* and *in vivo*, we reasoned
92 that MCT1 and MCT4-mediated lactate export might contribute to EBV-mediated B-cell
93 tumorigenesis, and virus-associated lymphoma cell growth more broadly. To address this, we
94 measured changes in lactate concentration and MCT expression through EBV-mediated B-cell
95 outgrowth and perturbed MCT1 and MCT4 function with small molecule antagonists. Our data
96 identify metabolic vulnerabilities that we propose could be exploited for the treatment of viral-
97 associated cancers.

98

99 **RESULTS**

100 **EBV infection of human B cells leads to an increase in lactate accumulation, secretion,**
101 **and the lactate transporter MCT1.** We and others have previously demonstrated that EBV
102 infection of primary human B cells leads to upregulation of glycolysis as evidenced by an increase
103 in glycolytic enzymes and the extracellular acidification rate (ECAR)(3, 10). To determine whether
104 the increase in ECAR was indicative of an increase in lactate export from infected cells, we
105 harvested media from EBV-infected primary human B cells at several time points following
106 infection and measured media lactate. We found that media lactate levels increased steadily after
107 infection as cell proliferation initiated by day 4 and through long-term outgrowth (day 35 =
108 lymphoblastoid cell line, or LCL) (**Fig. 1A**). However, we did not observe a concomitant rise in
109 intracellular lactate until late times post infection (**Fig. 1B**). This finding led us to assess the
110 mechanism of lactate secretion during early infection.

111 Under normal physiological conditions in most cells, lactate transport is mediated by the
112 monocarboxylate transporter 1 (MCT1). We found that while resting B cells had little MCT1
113 expressed at the RNA or protein level, by day 7 EBV-infected B cells were expressing high levels
114 of MCT1 that persisted through LCL outgrowth (**Fig. 1C-D**). MCT1 is a known transcriptional target

115 of c-Myc, which is transcriptionally regulated upon EBV infection by the latency protein EBV
116 Nuclear Antigen 2 (EBNA2)(33). To test the hypothesis that EBNA2 is the viral protein responsible
117 for MCT1 induction, we utilized the P493-6 model of regulated EBNA2 expression(34). In this
118 system, an endogenous EBNA2 is regulated post-translationally by β-estradiol due to its fusion to
119 the estrogen receptor. Loss of EBNA2 in this system in the absence of β-estradiol led to a loss
120 of MCT1 as well as c-Myc mRNA and protein and the mRNA of two other EBNA2 and c-Myc
121 targets, HES1 and MTHFD2 (**Fig. 1E-I**) (10, 35). Similarly, turning EBNA2 back on in these cells
122 led to re-expression of these targets.
123
124 **MCT1 inhibition causes growth arrest and increased lactate in early EBV-infected B cells.**
125 The induction of MCT1 expression early after EBV infection led us to ask whether MCT1 was
126 crucial for maintaining EBV-infected B-cell proliferation or survival given the known detrimental
127 consequences of lactate accumulation(13). To assess this, we used the MCT1 inhibitor,
128 AZD3965, which is currently in clinical trials for MCT1-overexpressing lymphomas(31). We
129 treated EBV-infected peripheral blood mononuclear cells (PBMCs) concurrent with infection and
130 assessed CD19+ B-cell proliferation by flow cytometry using the proliferation tracking dye
131 CellTrace Violet at different days post infection. We found that treatment with AZD3965 led to a
132 dose-dependent decrease in B-cell proliferation on days 4 and 7 post EBV infection, accompanied
133 by an increase in intracellular lactate levels (**Fig. 2A-C**). This effect on proliferation was due to a
134 G1/S phase growth arrest and not to increased B-cell death (**Supp. 1**). However, this effect was
135 lost by 14 days post infection and later in immortalized LCLs, suggesting an acquired resistance
136 to MCT1 inhibition (**Fig. 2D-E**).
137
138 **EBV-infected B cells acquire resistance to MCT1 inhibition during B-cell transformation**
139 **through induction of MCT4.** Given the fact that our data indicate a significant increase in
140 intracellular lactate concentrations in LCLs compared to early-infected B cells, we hypothesized

141 that EBV immortalization might induce the expression of another lactate exporter, which would
142 mitigate the effects of MCT1 inhibition. We found that expression of the MCT1 family member,
143 MCT4, significantly increased between days 7 and day 14 post-EBV infection (**Fig. 3A-C**).
144 Interestingly, this time period correlates with a known switch in the EBV latency gene expression
145 program from latency IIb (EBNAs only - EBNA1, 2, 3A, 3B, 3C, and LP) to latency III (EBNAs and
146 LMPs – LMP1, LMP2A/B). Indeed, LMP1 expression within LCLs correlated with MCT4, but not
147 MCT1 or MCT2 expression (**Fig. 3D**). Furthermore, MCT4 was found to be upregulated by LMP1
148 in a publicly available RNA-Seq dataset of LMP1-expressing DG75, EBV-negative Burkitt
149 lymphoma cells (**Fig. 3E**). Thus, the switch to latency III and expression of the viral protein LMP1
150 leads to B-cell induction of MCT4 that may help compensate for elevated glycolysis in EBV-
151 infected cells as they progress to become LCLs.
152
153 **Dual MCT1/4 inhibition suppresses LCL growth and sensitizes to killing by ETC inhibitors.**
154 The unique expression profile of MCT1 with MCT4 at later stages of EBV-mediated B-cell
155 outgrowth along with the significant accumulation of lactate in LCLs, led us to hypothesize that
156 MCT4 might play a critical role in LCL growth. To assess the role of MCT4 in LCLs, we took
157 advantage of a novel, low-nanomolar MCT4 inhibitor, VB124, which displays >1,000-fold
158 selectivity over MCT1(36). Much to our surprise, MCT4 inhibition had no observed effect on LCL
159 growth or viability (**Fig. 4A**). However, we reasoned that though MCT4 expression was unique to
160 LCLs during EBV-mediated B-cell outgrowth, perhaps the presence of MCT1 in LCLs rendered
161 them resistant to singular MCT4 inhibition. To test this, we treated LCLs with both AZD3965 (1
162 μM) and VB124 (20 μM) and monitored cell proliferation. Dual inhibition of MCT1 and MCT4 led
163 to a significant decrease in LCL growth, accompanied by a four-fold increase in intracellular
164 lactate (**Fig. 4B, C**). Similar to the MCT1 inhibition effect on early-infected B-cell proliferation,
165 MCT1/4 combined inhibition led to growth arrest in LCLs rather than cell death (**Supp. Fig 2**).

166 Treatment with exogenous L-lactate phenocopied dual MCT1/4 inhibition suggests a direct role
167 for lactate accumulation in the regulation of EBV-immortalized LCL growth (**Supp. Fig 3**).
168 We next sought to assess whether MCT inhibition might also render LCLs susceptible to
169 arrest or killing by electron transport chain (ETC) inhibitors as this therapeutic strategy has been
170 successful in other cancer models(30, 37). Indeed, LCLs were 20-fold more susceptible to the
171 complex I inhibitor phenformin (IC_{50} from ~100μM to ~5μM) when coupled with growth inhibitory
172 concentrations of AZD3965 (1μM) and VB124 (20 μM) (**Fig. 4D**). Moreover, treatment of LCLs
173 with 10 μM phenformin induced significantly more cell death in MCT1/4-inhibited cells than alone
174 (**Fig. 4E**). This increased cell death was accompanied by increased intracellular lactate levels as
175 well (**Fig. 4F**). Finally, we found that MCT1/4 inhibition also sensitized LCLs to killing by the FDA-
176 approved ETC inhibitor, metformin (**Fig. 4G-H**). These experiments support our hypothesis that
177 lactate accumulation in EBV-infected cells renders them hyper-sensitive to the ETC inhibitors
178 phenformin and metformin.
179
180 **Dual inhibition of MCT1/4 in LCLs compromises OCR and NAD^+/NADH ratios, and induces**
181 **oxidative stress.** We next sought to explore the mechanisms responsible for the sensitivity of
182 LCLs to MCT inhibition. We performed Seahorse assays on LCLs treated with MCT1 and 4
183 inhibitors for 24 hours. As expected, dual MCT1/MCT4 inhibition, which induced lactate
184 accumulation in LCLs, significantly decreased extracellular acidification (**Fig. 5A**). Unexpectedly,
185 however, dual MCT1/4 inhibition significantly decreased oxygen consumption rates (OCR) after
186 just 24 hours of treatment indicating that these metabolic changes precede the growth arrest
187 observed at later time points (**Fig. 5B**). This effect was even more pronounced with the addition
188 of phenformin, which was expected given the unequivocal role of the ETC on mitochondrial
189 respiration (**Fig. 5B**).

190 The production of lactate during glycolysis is coupled with the regeneration of NAD^+ from
191 NADH. Therefore, we assessed the NAD^+/NADH ratio in MCT1/4 inhibited LCLs. We found that
192 treated cells had a significantly lower NAD^+/NADH ratio than control LCLs (**Fig. 5C**). Since
193 NAD^+/NADH ratios directly contribute to the redox state of the cell, we investigated whether
194 compromised NAD^+/NADH levels in MCT1/4-inhibited LCLs could be inducing oxidative stress.
195 Using the reactive oxygen species (ROS)-sensitive fluorescent DCFDA dye, we found that ROS
196 levels increased significantly upon MCT1/4 inhibition (**Fig. 5D**). Furthermore, metabolite tracing
197 experiments using heavy-labeled ^{13}C-glucose indicated that dual MCT1/4 inhibition increased the
198 fractional contribution of glucose in reduced and oxidized glutathione (**Fig. 5F,H**). Furthermore,
199 the marked decrease in glutathione pools by 72 hours post-treatment suggests an effort to
200 mitigate accumulating ROS levels through glutathione antioxidant activity (**Fig. 5G,I**)
201
202 **EBV+ and KSHV+ lymphoma cell lines are sensitive to dual MCT1/4 and ETC inhibitors.**
203 EBV is an etiologic factor in the development of B-cell lymphomas of the immune suppressed
204 such as HIV-associated diffuse large B-cell lymphomas (DLBCL) and post-transplant
205 lymphoproliferative disease (PTLD)(38–40). Therefore, we asked whether the novel approach of
206 dual MCT1/4 inhibition in EBV-immortalized LCLs could also be effective in EBV-positive
207 lymphoma cells. We treated the EBV+ AIDS-immunoblastic lymphoma cell line, IBL-1, which like
208 LCLs, expresses MCT1 and MCT4, with both MCT1/4 inhibitors (**Fig. 6C**). We observed a striking
209 diminution in growth, similar to the phenotype in LCLs (**Fig. 6A**). Consistently, we also observed
210 synergy between MCT1/4 antagonism and metformin as well as phenformin in IBL-1 cells, which
211 supports a novel therapeutic approach to EBV+ lymphomas (**Fig. 6A and 6B**).
212 Given the robustness of this strategy, we asked whether other viral lymphomas may be
213 susceptible to MCT antagonism and combination with metformin. Kaposi Sarcoma Herpesvirus
214 (KSHV) is a closely related oncogenic gamma herpesvirus to EBV and is the etiologic agent of
215 Kaposi Sarcoma as well as primary effusion lymphomas (PEL) in HIV-infected individuals. First,

216 we confirmed expression of MCT1 and MCT4 in the PEL cell lines BCBL-1, VG-1, and BCLM,
217 alongside IBL-1 and LCLs (**Fig. 6C**). Then, we investigated whether dual MCT1/4 inhibition could
218 impact PEL growth, especially when combined with metformin, as was true in LCLs and IBL-1
219 cells. Consistent with our observation in EBV-infected cells, we observed that dual inhibition of
220 MCT1 and 4 uniformly suppressed growth of KSHV-infected PEL cells. Furthermore, MCT1/4
221 antagonism also increased sensitivity of PEL cells to metformin-mediated growth inhibition,
222 thereby expanding the applicability of this strategy to KSHV+ lymphomas (**Fig. 6D**).

223 **DISCUSSION**

224 Epstein-Barr virus reorganizes B-cell metabolic pathways to promote immortalization as a
225 precursor to the development of lymphomas in the immune suppressed. We and others have
226 previously described a balanced upregulation of oxidative phosphorylation and glycolysis through
227 EBV-mediated B-cell outgrowth(3, 10). In order to maintain glycolytic flux during aerobic
228 glycolysis, EBV-infected B cells must upregulate lactate transporters. In this study, we identified
229 an EBNA2/c-Myc mediated upregulation of MCT1 that was important for supporting increased
230 glycolysis during the hyper-proliferative burst early after EBV infection. However, infected cells
231 became resistant to MCT1 antagonism between one- and two-weeks post infection and we
232 observed a strong upregulation of MCT4. This correlated with the switch in viral latency programs
233 in which the viral LMP1 protein promoted MCT4 expression. EBV-immortalized lymphoblastoid
234 cell lines were sensitive to the inhibition of both MCT1 and MCT4 with specific small molecule
235 antagonists, which led to their growth arrest due to a loss in the oxygen consumption rate, an
236 accumulation of both lactate and reactive oxygen species, and depletion of NAD^+ relative to
237 NADH. Importantly, MCT1/4 inhibition rendered LCLs vulnerable to the inhibition of the electron
238 transport chain with phenformin or metformin. This synergistic effect on LCLs was also manifested
239 in lymphoma cell lines harboring EBV and also a related oncogenic gammaherpesvirus, KSHV,
240 suggesting a novel strategy for targeting viral-induced cancers.

241 The role of monocarboxylate transporters (MCTs) has been well studied in cancer, but not
242 during viral infection. The metabolic requirements of both processes are similar with a goal of
243 ramping up anabolic processes to either promote proliferation or viral particle production. Latent
244 oncogenic herpesviruses are unique in that they express specific proteins and non-coding RNAs
245 that reprogram cellular transcription and metabolic pathways, with the goal of promoting viral
246 genome replication during host cell proliferation. For example, during KSHV lytic replication,
247 glycolysis is required for maximal virion production, while during latent infection, 10 out of the 12
248 microRNAs are sufficient to induce glycolysis, thereby contributing to infected cell growth (41, 42).
249 KSHV-associated PEL also display elevated aerobic glycolysis and fatty acid biosynthesis
250 compared to primary B cells, highlighting the importance of these pathways in KSHV-associated
251 tumors, and another parallel between KSHV infection and tumorigenesis(43),(44). Similarly, the
252 EBV oncoprotein LMP1 upregulates glucose import through NFκB signaling to promote cell
253 survival(8). Thus, EBV and KSHV coordinately activate their infected cells in a similar manner to
254 how cellular oncogenes cooperate to reprogram metabolism in cancer. While both EBV and
255 KSHV-associated lymphomas display increased extracellular acidification rates (ECAR) and
256 lactate export due to increased glycolysis, only a handful of studies have addressed lactate
257 transporters in these cancers(9, 45). In one study, MCT4 RNA was shown to be upregulated in
258 EBV-immortalized LCLs relative to mitogen-activated B cells and freshly EBV-infected B cells, but
259 mainly due to its association with the induction of hypoxia(9, 46). More indirectly, KSHV-infected
260 PEL chemoresistance to doxorubicin and paclitaxel has been linked to expression of the MCT1/4-
261 associated chaperone glycoprotein Emmprin, which is regulated by the KSHV-encoded latency-
262 associated nuclear antigen (LANA) in KSHV+ PEL cell lines (47),(48). Given the similarities
263 between EBV and KSHV-mediated reprogramming of host metabolism, and based on our
264 observation that KSHV+ PELs arrest upon treatment with both MCT1/4 inhibitors, it is therefore
265 possible that both viruses require and/or regulate MCT1/4-mediated lactate export in similar ways.
266 Future studies would need to elucidate whether MCT1/4-mediated lactate transport in KSHV+

267 lymphomas is intertwined with other aspects of metabolism like redox regulation and oxidative
268 stress mitigation, as is the case in EBV-immortalized LCLs.

269 During EBV infection, the EBV master transcriptional regulator EBNA2 can both directly
270 and indirectly influence host metabolic pathways such as one-carbon metabolism and fatty acid
271 biosynthesis through c-Myc(10, 49). We find that concomitant induction of MCT1 through c-Myc
272 is critical to support continued proliferation as lactate is generated through glycolysis.
273 Interestingly, we found that early-infected cells were exquisitely sensitive to MCT1 inhibition
274 through AZD3965 with low nanomolar (~1-10 nM) concentrations halting growth while in many
275 other tumor cell systems 250 nM is typically used. This suggests that MCT1-mediated lactate
276 export could be particularly important for B-cell growth in the absence of MCT4 – a gene
277 expression signature which has also been observed in germinal center B cells(32).

278 We were intrigued by the finding that EBV-infected B cells became resistant to MCT1
279 inhibition between one and two weeks after infection as this is the timeframe when infected cells
280 switch from proliferation driven by the viral EBNA proteins (latency IIb) to that of the EBNAs and
281 the LMPs (latency III)(5, 6). Given this relationship and the prior knowledge that MCT4 induction
282 could promote resistance to MCT1 antagonism, we interrogated MCT4 upregulation and
283 sensitivity to a novel MCT4 inhibitor. Our data support the upregulation of MCT4 by LMP1, which
284 is also supported by a published data set of LMP1 expression in DG75 cells(50). Moreover, that
285 study found that LMP1 targets dependent on the metabolic and DNA damage regulator, PARP1,
286 were largely enriched in HIF1α targets. In fact, their data using the PARP1 inhibitor olaparib
287 suggests that LMP1 induction of MCT4 was PARP1-dependent. These data also nicely dovetail
288 with that of a previous study supporting the stabilization of HIF1α and its targets in EBV-infected
289 cells supported a “pseudo-hypoxia” that appears to be induced by EBV(9).

290 The mechanism of growth arrest mediated by MCT1/4 antagonism involved a reduction in
291 the extracellular acidification rate due to the accumulation of lactate within cells, but surprisingly
292 also, a significant reduction in the oxygen consumption rate (OCR). Moreover, these effects were
293 observed within 24 hours following treatment, preceding cellular growth arrest which occurs
294 between 48-72 hours after treatment. We were intrigued by the significant decrease in OCR upon
295 dual MCT1/4 inhibition, given that previous reports describe increased OCR upon lactate export
296 inhibition as a means of compensating for reduced glycolysis with increased OXPHOS (20,
297 22),(51, 52). One possible explantion for this observed decrease in OCR could be due to the
298 altered redox balance via depleted NAD+/NADH, which could inhibiting NADH:ubiquinone
299 oxidoreductase activity in complex I of the ETC(53). Another possibility might be due to the
300 observed defect in *de novo* pyrimidine metabolism, as dihydroorotate dehydrogenase (DHODH)
301 function is directly linked to complex III activity(54). Either way, the reduction of OCR upon
302 selective MCT1/4 inhibition in LCLs points at a unique vulnerability that can be further exploited
303 for therapeutic benefit in EBV-driven lymphomas in combination with ETC inhibitors like
304 metformin. Recently, dual MCT1/4 inhibition using the anti-hypertensive drug syrosingopine was
305 found to be synthetically lethal with metformin in leukemia and breast cancer cell lines due to
306 depleted NAD^+/NADH ratios(30). Interestingly, we found that in LCLs, selective inhibition of both
307 MCT1 and MCT4 with AZD3965 and VB124 was sufficient to significantly deplete NAD^+/NADH
308 ratios, while addition of the metformin analog phenformin did not further deplete these ratios (not
309 shown). This therefore suggests an alternative mechanism of metformin/phenformin-induced
310 killing in MCT1/4-inhibited cancer cells, not directly related to NAD+/NADH metabolism.

311 The MCT1 inhibitor AZD3965 is currently in clinical trials for various lymphomas and solid
312 tumors(31). However, no such trials exist for MCT4, primarily due to the lack of MCT4-specific
313 inhibitors. While pan-MCT1/4 inhibitors do exist, these also target other metabolic pathways such
314 as the glycolytic enzyme enolase, and mitochondrial pyruvate transport in addition to MCT1 and

315 MCT4, which can produce adverse side effects(55, 56). Using the novel MCT4-specific inhibitor
316 VB124 as a tool compound, we were able to explore the therapeutic potential of MCT1/4-targeted
317 combination therapy in viral-associated lymhpomas. We recognize that pre-clinical testing of
318 AZD3965 and VB124 in primary cells and cell lines may be an incomplete representation of
319 lymphomagenesis *in vivo* as contributions from the tumor microenvironment are lacking.
320 However, EBV has a narrow host tropism and is unable to infect mice or other common small
321 animal models. Recent development of humanized mouse models of EBV infection will be useful
322 in assessing how metabolic pathways like MCT1/MCT4-mediated lactate transport contribue to
323 EBV-driven tumorigenesis *in vivo*(57).

324 **MATERIALS AND METHODS**

325 **Cell lines, culture conditions, and viruses**

326 Buffy coats were obtained from normal human donors through the Gulf Coast Regional
327 Blood Center (Houston, TX) and peripheral blood mononuclear cells (PBMCs) were isolated by
328 Ficoll Histopaque-1077 gradient (Sigma, H8889). B95-8 strain of Epstein-Barr virus was produced
329 from the B95-8 Z-HT cell line as previously described (52). Virus infections were performed in
330 bulk by adding 50 µL of filtered B95-8 supernatant to $1x10^6$ PBMCs.

331 All LCLs were kept in RPMI 1640 medium supplemented with 10% heat-inactivated fetal
332 bovine serum (Corning), 2 mM L-Glutamine, 100 U/ml penicillin, 100 µg/ml streptomycin
333 (Invitrogen), and 0.5 µg/mL Cyclosporine A (Sigma). The same conditions were used for the EBV−
334 germinal-center-derived B-cell lymphoma line BJAB (obtained from George Mosialos, Aristotle
335 University, Thessaloniki, Greece). Kaposi's sarcoma-associated herpesvirus-positive
336 (KSHV+)/EBV− primary effusion lymphoma (PEL) cell lines VG-1, BCLM, and BCBL1 were
337 provided by Dirk Dittmer (University of North Carolina [UNC], Chapel Hill, NC) or Bryan Cullen
338 (Duke University, Durham, NC) with permission from the original authors and kept in RPMI 1640

339 medium supplemented with 15% fetal bovine serum, 10 mM HEPES, 1 mM sodium pyruvate, and
340 0.05 mM β-mercaptoethanol (Sigma). The EBV-positive cell line derived from an AIDS
341 immunoblastic lymphoma, IBL-1, was kindly provided by Ethel Cesarman (Weill Cornell Medical
342 College, New York, NY) and kept in RPMI 1640 supplemented with 20% fetal bovine serum.
343 P493-6 cells (a kind gift of Dr. Georg Bornkamm, Helmholtz Zentrum München) were cultured in
344 RPMI 1640 supplemented with 10% tetracycline-free FBS (Hyclone SH30070), 1 μM β-Estradiol,
345 and 1 μg/mL Tetracycline. P493-6 cells were washed three times with β-Estradiol-free media, and
346 then cultured in the absence of β-Estradiol for 3 days to induce the EBNA2-OFF state. After
347 washing 3 times, the cells were then cultured again for 3 days upon reintroducing 1 uM β-
348 Estradiol, returning P493-6 cells to the EBNA2-ON state. All cells were cultured at 37°C in a
349 humidified incubator at 5% CO2.

350 **Flow cytometry and sorting**

351 To track proliferation in EBV-infected B cells, cells were stained with CellTrace Violet
352 (Invitrogen, C34557), a fluorescent proliferation-tracking dye. Cells were first washed in FACS
353 buffer (5% FBS in PBS), stained with the appropriate antibody for 30min-1hr at 4°C in the dark,
354 and then washed again before being analyzed on a BD FACS Canto II. Proliferating infected B
355 cells were sorted to a pure population of CD19+/CellTrace Violet on a MoFlo Astrios Cell Sorter
356 at the Duke Cancer Institute Flow Cytometry Shared Resource. Mouse anti-human CD19
357 antibody (Biolegend Cat# 152410) conjugated with APC was used as a surface B-cell marker in
358 flow cytometry.

359 **Cell Growth Assays**

360 LCLs were seeded at a density of $3x10^5$ cells/mL, and treated with either DMSO, AZD3965
361 (Cayman Chemicals), VB124 (a kind gift of Mark Parnell, Vettore LLC), phenformin (Cayman
362 Chemicals), or metformin (Cayman Chemicals) for one to four days. VB124 required

363 concentrations much higher than its IC50 (8.6 nM) in serum due to high(~99%) serum protein
364 binding common for carboxylic acids like VB124. Drug treatments were normalized across
365 conditions to contain 0.01% DMSO. Cell growth was assessed daily by either CellTiter Glo
366 (Promega) or counting by Trypan exclusion on an automated cell counter (Countess II,
367 ThermoFisher). Luminescence was measured using a microplate reader (Biotek Synergy HTX).

368 **Gene Expression Analysis**

369 Total RNA was isolated from cells by using a Qiagen RNeasy kit and then reverse transcribed to
370 generate cDNA with the High Capacity cDNA kit (Applied Biosystems). Quantitative PCR was
371 performed by using SYBR green (Quanta Biosciences) in an Applied Biosystems Step One Plus
372 instrument. Primer sets include MCT1 (**F:** GACCTTGTTGGACCCCAGAG,
373 **R**:AGCCGACCTAAAAGTGGTGG), MCT4 (**F:** AGGTCTACCTCACCACTGGG, **R**:
374 CACAGGAAGACAGGGCTACC.

375 **BrdU Staining**

376 Cell cycle progression was assessed by BrdU staining. Infected PBMCs treated with DMSO, Chk2
377 inhibitor II (EMD Millipore), or AZD3965 (Cayman Chemicals) cells were stained with CD19, and
378 pulsed with BrdU (BD Biosciences, Cat# 552598) for two hours following fixation and
379 permeabilization. Afterwards, cells were treated with a DNAse to expose BrdU-bound epitopes,
380 and stained wth a BrdU-fluorescent antibody as well as the total DNA and cell death marker 7-
381 AAD. Then, BrdU and 7-AAD fluorescence values were acquired on a flow cytometer (FACS
382 Canto II).

383 **Immunoblotting**

384 Cells were pelleted and washed in PBS, and then lysed in LDS Sample Buffer (NuPAGE) with
385 complete protease inhibitors. All protein lysates were run on NuPage 4–12% gradient gels

386 (LifeTechnology) and transferred to PVDF membrane (GE Healthcare). Membranes were blocked
387 in 5% milk in TBST and stained with primary antibody overnight at +4°C, followed by a wash and
388 staining with secondary HRP-conjugated antibody for 1 hour at room temperature. Antibodies
389 include MCT1 (Abcam, Cat# ab85021, 1:1000 dilution), MCT4 (Proteintech, Cat# 22787-1-AP,
390 1:1000 dilution), LMP1 (S12; gift from Elliot Kieff, Harvard Medical School), c-Myc (Santa Cruz
391 Biotechnology, SC-764), EBNA2 (PE2; gift from Elliot Kieff), MAGOH (Santa Cruz, SC-56724).
392 We use MAGOH as a loading control because it does not change in expression from resting B
393 cells through LCL outgrowth.

394 **Seahorse Analysis**

395 Extracellular acidification rate (ECAR) and oxygen consumption rate (OCR) were measured using
396 the Seahorse XFe96 extracellular flux analyzer (Agilent Technologies) Cell Energy Phenotype
397 Test. LCLs were attached to culture plates by using Cell-Tak (BD Bioscience). ECAR and OCR
398 were measured in Seahorse XF Base Medium supplemented with 1 mM pyruvate, 2 mM
399 glutamine, and 10 mM glucose (Sigma Aldrich). ECAR and OCR values were normalized to cell
400 number. For stress measurements, ECAR and OCR were measured over time after injection of
401 oligomycin and FCCP.

402 **^{13}C-glucose Tracing**

403 Glucose tracing experiments were performed using ^{13}C6-glucose (Cambridge Isotope
404 Laboratories Cat. CLM-1396-PK). LCLs were cultured in glucose-free RPMI supplemented with
405 10mM ^{13}C6-glucose and 10% dialyzed FBS, seeded at a density of 300,000 LCLs/mL and treated
406 with either DMSO or 1μM AZD3965 + 20μM VB124 for 48 or 72 hours. Then cells were harvested
407 and washed twice with ice-cold PBS, followed by metabolite extraction with ice-cold 80%
408 methanol in deionized water, and evaporation for approximately two hours. Dried metabolites
409 were reconstituted in 100 μL of a 50% acetonitrile(ACN) 50% dH20 solution. Samples were

410 vortexed and spun down for 10 min at 17,000g. 70 µL of the supernatant was then transferred to
411 HPLC glass vials. 10 µL of these metabolite solutions were injected per analysis. Samples were
412 run on a Vanquish (Thermo Scientific) UHPLC system with mobile phase A (20mM ammonium
413 carbonate, pH 9.7) and mobile phase B (100% ACN) at a flow rate of 150 µL/min on a SeQuant
414 ZIC-pHILIC Polymeric column (2.1 × 150 mm 5 µm, EMD Millipore) at 35°C. Separation was
415 achieved with a linear gradient from 20% A to 80% A in 20 min followed by a linear gradient from
416 80% A to 20% A from 20 min to 20.5 min. 20% A was then held from 20.5 min to 28 min. The
417 UHPLC was coupled to a Q-Exactive (Thermo Scientific) mass analyzer running in polarity
418 switching mode with spray-voltage=3.2kV, sheath-gas=40, aux-gas=15, sweep-gas=1, aux-gas-
419 temp=350°C, and capillary-temp=275°C. For both polarities mass scan settings were kept at full-
420 scan-range=(70-1000), ms1-resolution=70,000, max-injection-time=250ms, and AGC-
421 target=1E6. MS2 data was also collected from the top three most abundant singly-charged ions
422 in each scan with normalized-collision-energy=35. Each of the resulting ".RAW" files was then
423 centroided and converted into two ".mzXML" files (one for positive scans and one for negative
424 scans) using msconvert from ProteoWizard(58). These ".mzXML" files were imported into the
425 MZmine 2 software package(59). Ion chromatograms were generated from MS1 spectra via the
426 built-in Automated Data Analysis Pipeline (ADAP) chromatogram module and peaks were
427 detected via the ADAP wavelets algorithm(60). Peaks were aligned across all samples via the
428 Random sample consensus aligner module, gap-filled, and assigned identities using an exact
429 mass MS1(+/-15ppm) and retention time RT (+/-0.5min) search of our in-house MS1-RT
430 database. Peak boundaries and identifications were then further refined by manual curation.
431 Peaks were quantified by area under the curve integration and exported as CSV files. The peak
432 areas were additionally processed via the R package AccuCor to correct for natural isotope
433 abundance(61). Peak areas for each sample were normalized by the measured area of the
434 internal standard trifluoromethanesulfonate (present in the extraction buffer) and by the number
435 of cells present in the extracted sample.

436 **Lactate and NAD^+/NADH Measurements**

437 Intracellular and extracellular lactate concentrations were determined using the Lactate Glo
438 (Promega) assay kit. Briefly, cells were harvested and washed in ice cold PBS once, then
439 immediately inactivated with 0.6N HCl to halt metabolic activity and neutralized with 1M Tris base.
440 The resulting lysate was combined at a 1:1 ratio with the lactate detection reagent, and
441 luminescence measured a microplate reader. For intracellular lactate measurements involving
442 early-infection time points, PBMCs were first depleted for CD3+ T cells (RosetteSep™ Human
443 Granulocyte Depletion Cocktail), sorted to a pure population of CD19+ B cells on a MoFlo Astrios
444 Cell Sorter at the Duke Cancer Institute Flow Cytometry Shared Resource. Purified B cells were
445 either treated as indicated, or used as the starting cell population for time-course lactate
446 measurments. Mouse anti-human CD19 antibody (Biolegend Cat# 152410) conjugated with APC
447 was used as a surface B-cell marker in flow cytometry.

448 NAD^+/NADH ratios were measured using the NAD^+/NADH Glo assay (Promega)
449 according to the manufacturer's protocol. Briefly, harvested cells were washed in PBS, lysed with
450 Tris Base supplemented with 1% Dodecyl trimethylammonium bromide, treated with 0.4N HCl
451 (for NAD^+), and heated (for NADH) at 60°C for 15 min. Each sample was then added at a 1:1 ratio
452 with a luciferin detection reagent, and NAD^+ or NADH luminescence measured separately using
453 a BioTek Synergy™ 2 microplate reader.

454 **ROS Measurements**

455 ROS fluorescence was determined using the ROS-sensitive dye DCFDA (Cayman Chemicals Cat
456 #601520. Cells were pelleted and washed in the provided wash buffer, and then stained in 20μM
457 DCFDA for 1.5 hours at 37°C protected from light. Then, cells were washed once in the provided
458 wash buffer and FITC fluorescence measured in a flow cytometer. Pyocyanin (1mM) was used
459 as a positive control and N-acetylcysteine (300mM) as a negative control.

460 **ACKNOWLEDGMENTS**

461 This work was supported by National Institute of Health (NIH) grants R01-
462 CA140337 (to M.A.L.), T32GM007105-43, T32-CA009111 (to E.N.B.), T32CA009056 (to
463 J.C.), and R01 CA215185 (to H.R.C.) as well as RSG-16-111-01-MPC from the American
464 Cancer Society (to H.R.C.), the CDI Harry Winston Fellowship award (to J.C.), and the
465 St. Baldrick's Foundation Fellowship award (to J.C.). Additional funding came from the
466 Duke CFAR, and NIH-funded program (grant 5P30-Al064518).

467 The authors would like to thank Dr. Michael Cook, Nancy Martin, Lynn Martinek
468 and the Duke Cancer Institute Shared Flow Cytometry core facility for invaluable
469 assistance with flow cytometry and cell sorting. We would also like to thank Dr. Nancie
470 McIver and Amanda Nichols of the Duke Cellular Metabolism Analysis Core for their
471 guidance with the Seahorse XF anaysis. Finally, we would like to thank Ernst Schmid of
472 the UCLA Department of Biological Chemistry for assistance with mass spectrometry and
473 downstream analysis of isotopic tracing experiments.

474 **AUTHOR CONTRIBUTIONS**

475 M.A.L., E.N.B, J.E.M., J.M.C., H.R.C., and J.C. conceived and designed research
476 experiments. Specifically, M.A.L., J.E.M., and H.R.C. recognized that EBNA proteins may
477 regulate MCT1. J.E.M. with guidance from H.R.C. and J.C. initiated experiments on MCT1
478 regulation and function. J.E.M. trained E.N.B. in the laboratory with experimental
479 approaches on EBV-infection, drug treatments, and flow cytometry. E.N.B. and J.E.M.
480 performed buffy coat isolations from peripheral blood, EBV infections, and early-infection
481 treatment with AZD3965 and FACS analysis. E.N.B. performed all late-infection/LCL

482 treatments with MCT inhibitors, phenformin and metformin, lactate measurements,
483 Seahorse analysis, and metabolic assays. J.E.M. performed RNA-seq analysis, as well
484 as BrdU labeling. J.M.C. performed time-course qPCR experiments as well as all P493-
485 6 experiments. M.P. generously provided the MCT4 inhibitor VB124 and offered valuable
486 insight on experimental design of treatments in LCLs. J.C. and H.R.C. contributed to the
487 experimental design and execution of ^{13}C6-glucose tracing. E.N.B. and M.A.L. wrote and
488 all authors edited the manuscript.
489

490 **FIGURES AND FIGURE LEGENDS**

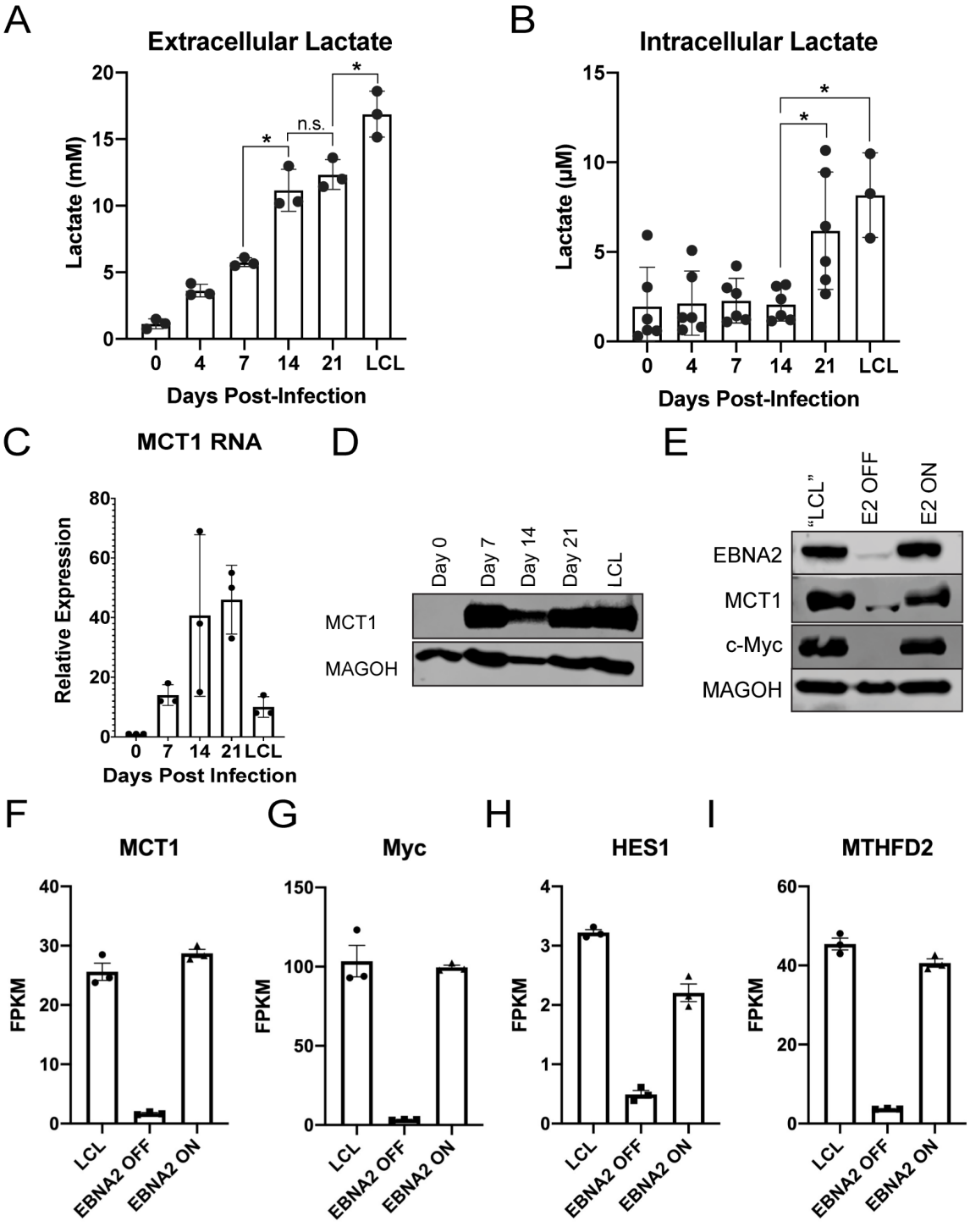

491

492 **Figure 1. EBV infection of human B cells leads to an increase in lactate transport**
493 **through MCT1.** ***A***. Extracellular (n=3) and ***B.*** Intracellular (n=6) lactate concentration
494 during EBV-infected B-cell immortalization. Extracellular concentration was obtained from
495 the supernatant of CD19+ isolated B cells at a concentration of $1x10^6$/mL and corrected
496 to cell-free growth medium lactate concentrations. Intracellular lactate concentration is
497 per 12,500 cells. ***C.*** MCT1 RNA (n=3) and ***D.*** Representative protein levels during EBV-
498 infected B-cell immortalization. MAGOH is a loading control used because the expression
499 of this gene is not changed upon B-cell outgrowth. ***E.*** Immunoblot of EBNA2, MCT1, and
500 c-Myc in P493-6 cells at the "LCL" state with stable EBNA2 expression, EBNA2 OFF in
501 the absence of β-estradiol, and EBNA2 ON with EBNA2 expression regained. ***F-I.*** RNA-
502 Seq data showing MCT1, c-Myc. HES1, and MTHFD2 expression in P493-6 B cells (n=3).
503 FPKM= Fragments Per Kilobase of transcript per Million mapped reads. Statistical
504 significance determined by paired t-test. *=p<0.05, **=p<0.01, ***=p<0.001.

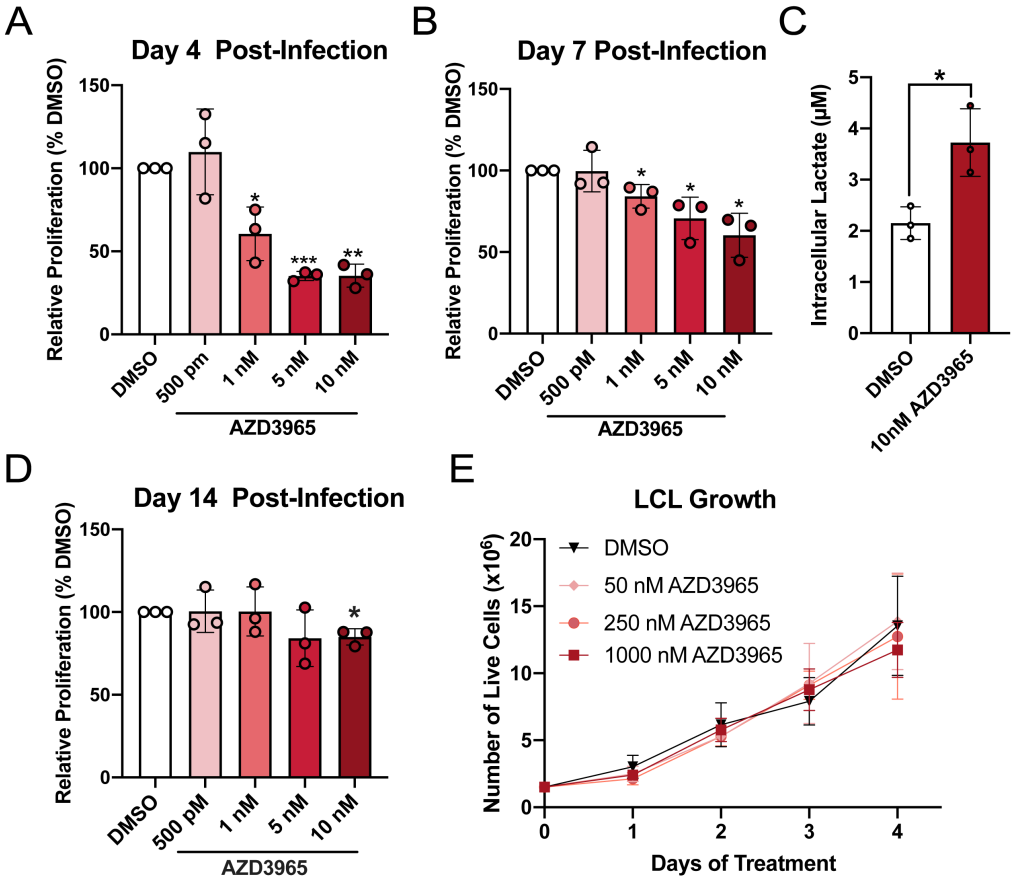

Figure 2. MCT1 inhibition leads to growth arrest and lactate buildup in early EBV-infected B cells. *A*. Bulk PBMCs (n=3) were treated with AZD3965 immediately following EBV infection, and CD19+ B-cell proliferation was determined by flow cytometry 4 days later. Cell counts were bead normalized. ***B.*** Bulk PBMCs (n=3) were treated 4 days post-infection, and CD19+ B-cell proliferation assessed by flow cytometry at 7 days post-infection. ***C.*** CD19-purified B cells (n=3) were treated at four days post-infection and intracellular lactate assessed three days later at seven days post-infection. ***D.*** Same as ***B***, except proliferation was assessed at 14 days post-infection. ***E.*** Growth curve of LCLs (n=3) treated with varying concentrations of AZD3965. LCL growth was determined by daily assessment of trypan blue exclusion. Statistical significance determined by paired t-test. *=p<0.05, **=p<0.01, ***=p<0.001.

517

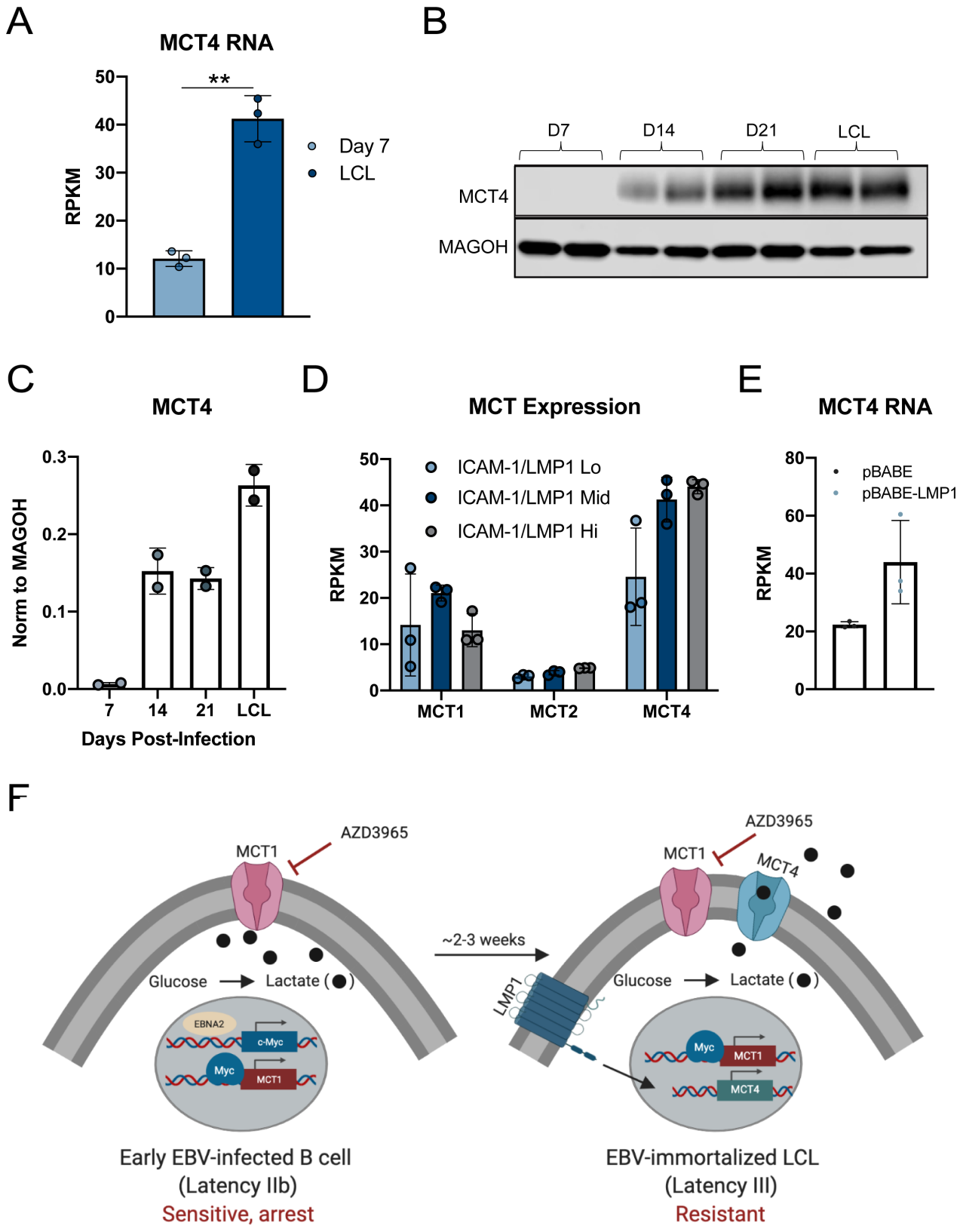
A
MCT4 RNA
**
RPKM
50
40
30
20
10
0
Day 7
LCL
B
D7
D14
D21
LCL
MCT4
MAGOH
C
MCT4
Norm to MAGOH
0.3
0.2
0.1
0.0
7
14
21
LCL
Days Post-Infection
D
MCT Expression
ICAM-1/LMP1 Lo
ICAM-1/LMP1 Mid
ICAM-1/LMP1 Hi
RPKM
50
40
30
20
10
0
MCT1
MCT2
MCT4
E
MCT4 RNA
pBABE
pBABE-LMP1
RPKM
80
60
40
20
0
F
AZD3965
MCT1
Glucose
Lactate
EBNA2
c-Myc
Myc
MCT1
~2-3 weeks
LMP1
AZD3965
MCT1
MCT4
Glucose
Lactate
Myc
MCT1
MCT4
Early EBV-infected B cell
(Latency IIb)
Sensitive, arrest
EBV-immortalized LCL
(Latency III)
Resistant

518

519 **Figure 3. EBV-infected B cells acquire resistance to MCT1 inhibition during B-cell**
520 **transformation due to MCT4 induction.** ***A.*** Queried RNA-Seq data of MCT4 expression
521 in EBV-infected B cells (n=3) at 7 days post-infection, and LCL(62). RPKM= Reads Per
522 Kilobase of transcript per Million mapped reads. ***B.*** Western blot of MCT4 in CD19+-
523 purified B cells during EBV-mediated B-cell immortalization. MAGOH= loading control. ***C.***
524 quantification of B (n=2). ***D.*** Monocarboxylate transporter (MCT) expression from RNA-
525 Seq of LCLs sorted by the LMP1 proxy, ICAM-1, status. ***E.*** Queried RNA-Seq data of
526 MCT4 expression in DG75 cells (n=3) transfected with LMP1. Statistical significance was
527 determined by paired t-test. *=p<0.05, **=p<0.01, ***=p<0.001. ***F***. Schematic representation
528 of MCT1 inhibitor sensitivity during EBV-mediated B lymphocyte immortalization.

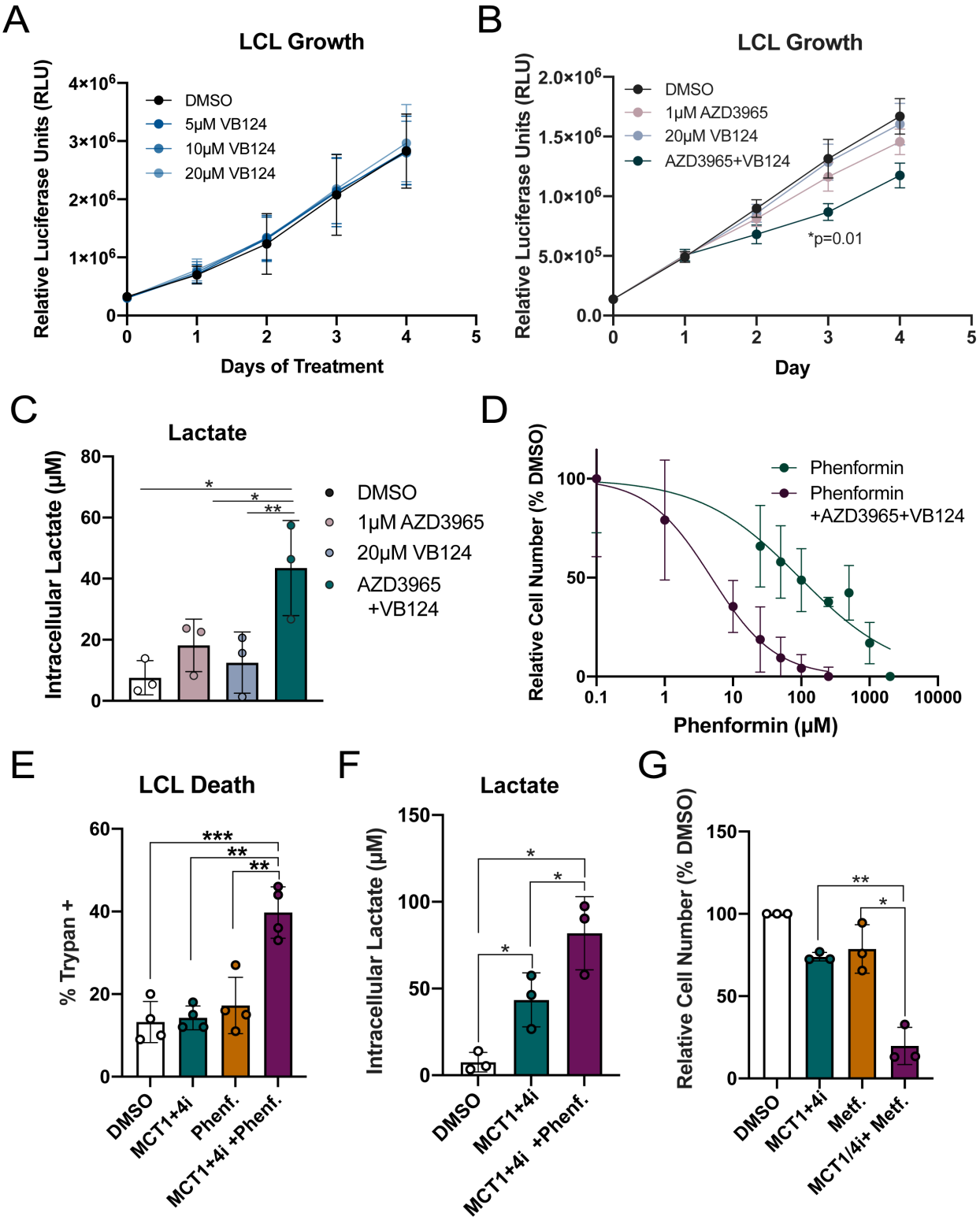

529

530 **Figure 4. Dual MCT1/4 inhibition sensitizes LCLs to killing by electron transport**

531 **chain (ETC) inhibitors.** ***A.*** Growth curve of LCLs (n=3) treated with varying

532 concentrations of VB124. Growth was determined by CellTiter Glo. ***B.*** Growth curve of
533 LCLs (n=3) treated with either DMSO, 1μM AZD3965, 20μM VB124, or 1μM AZD3965 +
534 20μM VB124. Growth was assessed as in A. ***C.*** Intracellular lactate concentration (per
535 12,500 cells), of LCLs (n=3) treated with either DMSO, 1μM AZD3965, 20μM VB124, or
536 1μM AZD3965 + 20μM VB124. ***D.*** Phenformin IC50 curve. Generated 72h after treatment
537 of LCLs (n=3) with either phenformin or 1μM AZD3965 + 20μM VB124. Relative cell
538 number was determined by CellTiter Glo luminescence. Values were normalized to
539 DMSO to obtain %DMSO. ***E.*** LCL death, as determined by trypan blue staining after 72h
540 of treatment. n=3. MCT1+4i= 1μM AZD3965 + 20μM VB124, Phenf. = 10μM Phenformin
541 ***F.*** Intracellular lactate concentration (per 12,500 cells), of LCLs treated for 3 days ***G.***
542 Relative LCL number as determined by CellTiter Glo, 72h after treatment. n=3. MCT1+4i=
543 1μM AZD3965 + 20μM VB124, Metf. = 2mM Metformin. Statistical significance was
544 determined by paired t-test. ***H.*** LCL death, based on trypan blue positivity, following 72h
545 of treatment. n=3. *=p<0.05, **=p<0.01, ***=p<0.001.

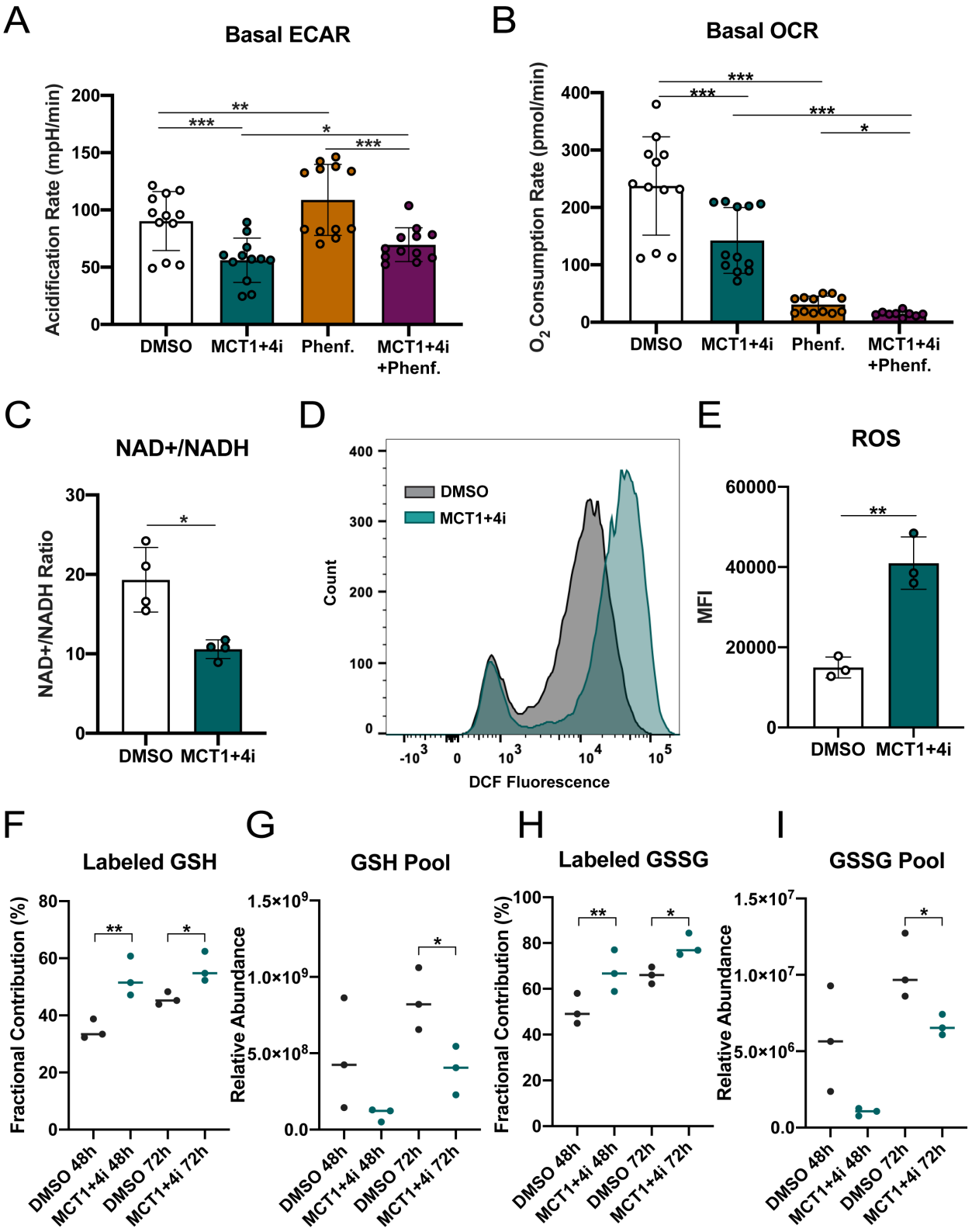
A
Basal ECAR
Acidification Rate (mpH/min)
200
150
100
50
0
**
***
*
***
DMSO
MCT1+4i
Phenf.
MCT1+4i +Phenf.
B
Basal OCR
O_2 Consumption Rate (pmol/min)
400
300
200
100
0
***
***
***
*
DMSO
MCT1+4i
Phenf.
MCT1+4i +Phenf.
C
NAD+/NADH
NAD+/NADH Ratio
30
20
10
0
*
DMSO
MCT1+4i
D
DMSO
MCT1+4i
Count
400
300
200
100
0
-10^3
0
10^3
10^4
10^5
DCF Fluorescence
E
ROS
MFI
60000
40000
20000
0
**
DMSO
MCT1+4i
F
Labeled GSH
Fractional Contribution (%)
80
60
40
20
0
**
*
DMSO 48h
MCT1+4i 48h
DMSO 72h
MCT1+4i 72h
G
GSH Pool
Relative Abundance
1.5×10^9
1.0×10^9
5.0×10^8
0.0
*
DMSO 48h
MCT1+4i 48h
DMSO 72h
MCT1+4i 72h
H
Labeled GSSG
Fractional Contribution (%)
100
80
60
40
20
0
**
*
DMSO 48h
MCT1+4i 48h
DMSO 72h
MCT1+4i 72h
I
GSSG Pool
Relative Abundance
1.5×10^7
1.0×10^7
5.0×10^6
0.0
*
DMSO 48h
MCT1+4i 48h
DMSO 72h
MCT1+4i 72h

546

547 **Figure 5. Dual inhibition on MCT1/4 in LCLs compromises OCR and NAD/NADH**
548 **ratios and induces oxidative stress.** ***A.*** Seahorse assay showing extracellular
549 acidification rate (ECAR) and ***B.*** Oxygen consumption rate (OCR) of LCLs (n=4) in
550 triplicate. MCT1+4i= 1μM AZD3965 + 20μM VB124. Phenf. = 10μM Phenformin. ***C.***
551 NAD^+/NADH ratio of LCLs (n=4) treated for 48h ***D.*** Fluorescence-activated cell sorting
552 (FACS) histograms of treated LCLs (n=3) stained with 2',7'-dichlorodihydrofluorescein
553 diacetate (H_2-DCFDA). ***E.*** Mean fluorescence intensity (MFI) of D. ***F-I.*** Metabolic analysis
554 with ^{13}C-6-glucose tracing of reduced (GSH) or oxidized (GSSG) glutathione in LCLs
555 (n=3) treated with either DMSO or MCT1+MCT4 inhibitors for 48h or 72h. Cells were
556 cultured in the presence of ^{13}C6-labeled glucose-supplemented RPMI medium. Fractional
557 contribution= % heavy-labeled GSH or GSSG relative to pool size. Pool= Relative
558 abundance of GSH or GSSH in sample, as determined by LC-MS. Statistical significance
559 was determined by paired t-test. *=p<0.05, **=p<0.01, ***=p<0.001.

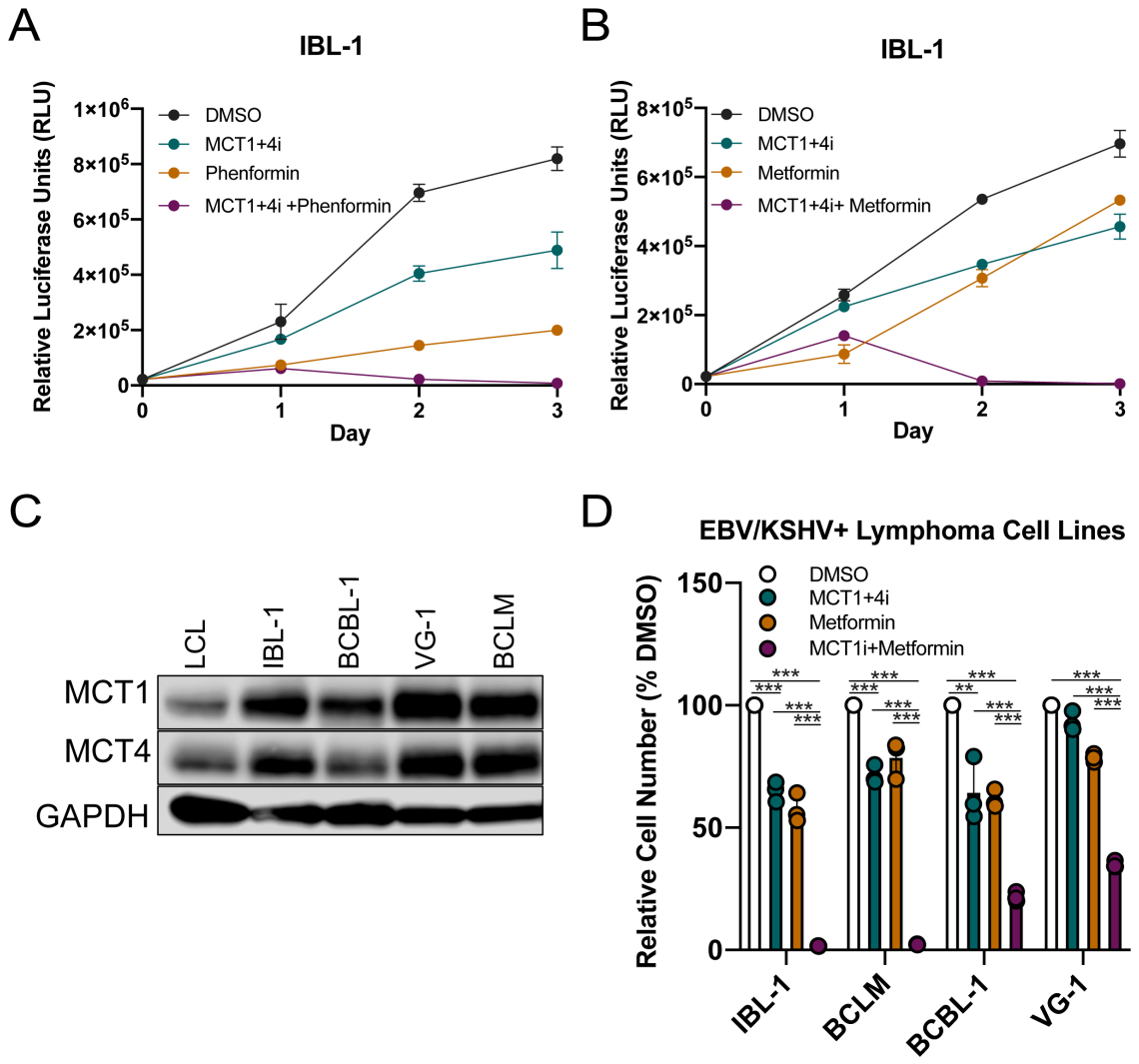

560

561 **Figure 6. EBV+ and KSHV+ lymphoma cell lines are sensitized to killing by**
562 **metformin upon dual MCT1/4 inhibition.** ***A, B.*** Growth over time of the EBV+ AIDS
563 immunoblastic lymphoma cell line IBL-1 (n=3), in the presence of both MCT1/4 inhibitors,
564 and ETC inhibitors metformin and phenformin. MCT1+4i= 1μM AZD3965 + 20μM VB124.
565 Phenformin= 100μM Metformin= 2mM. CellTiter Glo luminescence was used as proxy for
566 cell growth. ***C***. Immunoblot of MCT1 and MCT4 in EBV+ or KSHV+ primary effusion
567 lymphoma (PEL) cell lines, compared to EBV-immortalized LCLs. IBL-1= EBV+, KSHV-
568 AIDS immunoblastic lymphoma, BCBL-1= EBV-, KSHV+ PEL, VG-1= EBV-, KSHV+ PEL,

569 BCLM= EBV-, KSHV+ PEL. GAPDH= loading control. ***D.*** Relative cell count of
570 EBV+/KSHV+ lymphoma cell lines (n=3) 48h after treatment. Statistical significance was
571 determined by multiple t-test. *=p<0.05, **=p<0.01, ***=p<0.001.

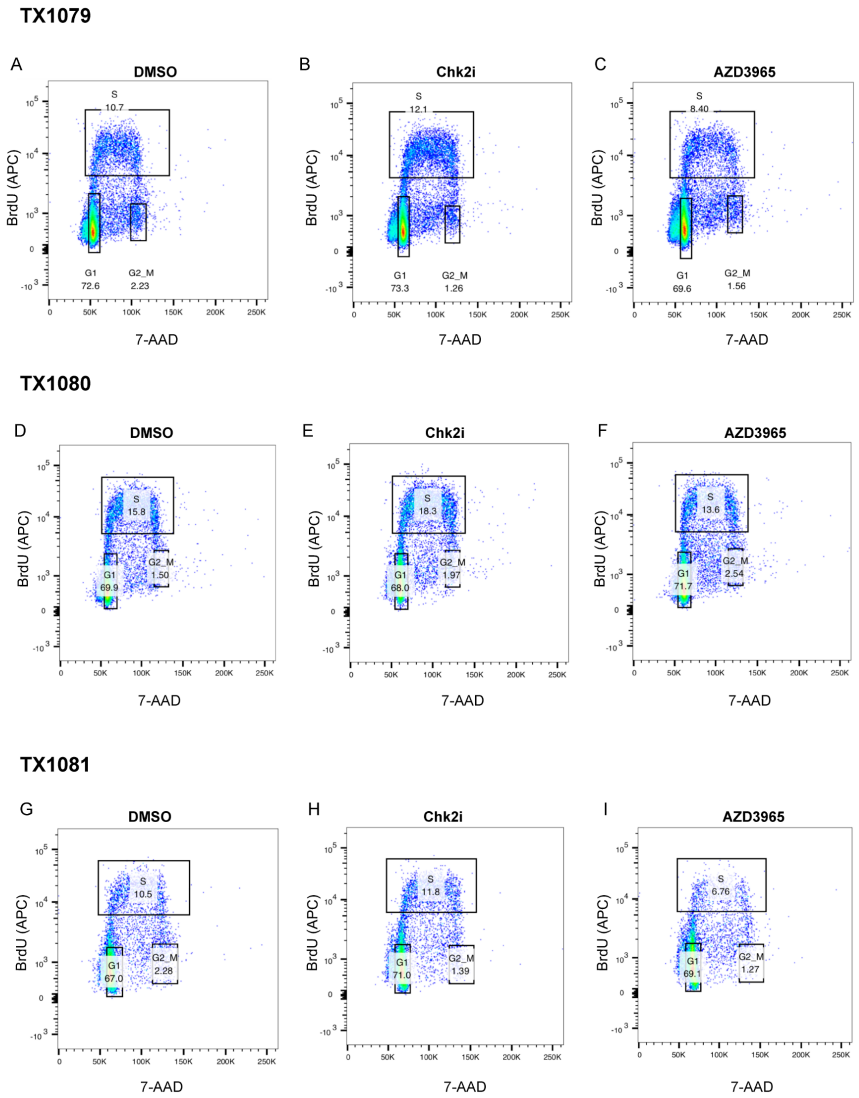

572

573 **Supplementary Figure 1. MCT1 inhibition in early EBV-infected B cells leads to a G1/S-**
574 **phase growth arrest, and not cell death.** ***A-I.*** Three PBMC donors were treated with either
575 DMSO, 5μM Chk2 inhibitor II, or 250nM AZD3965 for 48h. After 48h, cells were pulsed with BrdU
576 for 2h, and cell cycle progression assessed by flow cytometry. Chk2i = positive proliferation
577 control.

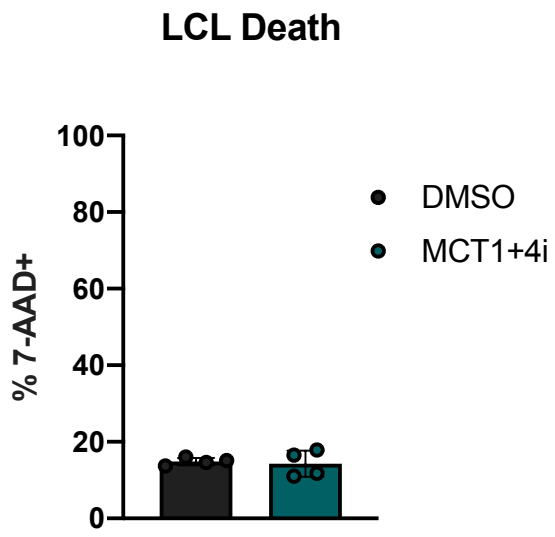

578

579 **Supplementary Figure 2. Dual MCT1/4 inhibition in LCLs does not result in cell death.** Two
580 LCL donors were treated in duplicate (n=4) with either DMSO or 1μM AZD3965 + 20μM VB124
581 for 72h, and 7-AAD positivity was assessed via fluorescence-activated cell sorting (FACS).

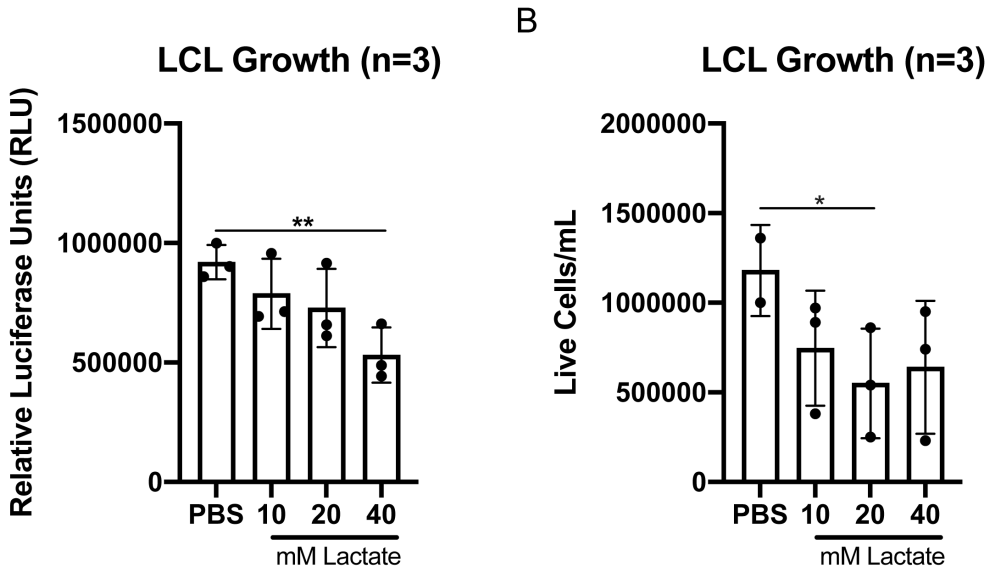

582

583 **Supplementary Figure 3. Exogenous L-lactate treatment in LCLs leads to growth arrest.**
584 LCLs were treated for 72h with varying concentrations of L-lactate. Growth was assessed by
585 either CellTiter Glo (***A***) or trypan blue exlusion counting (***B***). Statistical significance was
586 determined by paired t-test. *=p<0.05, **=p<0.01.

587 **REFERENCES**

588 1. G. J. Babcock, L. L. Decker, M. Volk, D. A. Thorley-Lawson, EBV Persistence in Memory B
589 Cells In Vivo. *Immunity* **9**, 395–404 (1998).

590 2. P. A. Nikitin, *et al.*, An ATM/Chk2-mediated DNA damage-responsive signaling pathway
591 suppresses Epstein-Barr virus transformation of primary human B cells. *Cell Host Microbe*
592 **8**, 510–522 (2010).

593 3. K. McFadden, *et al.*, Metabolic stress is a barrier to Epstein–Barr virus-mediated B-cell
594 immortalization. *Proc. Natl. Acad. Sci.* **113**, E782–E790 (2016).

595 4. C. Shannon-Lowe, A. B. Rickinson, A. I. Bell, Epstein–Barr virus-associated lymphomas.
596 *Philos. Trans. R. Soc. B Biol. Sci.* **372** (2017).

597 5. A. M. Price, M. A. Luftig, To Be or Not IIb: A Multi-Step Process for Epstein-Barr Virus Latency
598 Establishment and Consequences for B Cell Tumorigenesis. *PLOS Pathog.* **11**, e1004656
599 (2015).

600 6. J. E. Messinger, J. Dai, L. J. Stanland, A. M. Price, M. A. Luftig, Identification of Host
601 Biomarkers of Epstein-Barr Virus Latency IIb and Latency III. *mBio* **10** (2019).

602 7. P. A. Nikitin, A. M. Price, K. McFadden, C. M. Yan, M. A. Luftig, Mitogen-induced B-cell
603 proliferation activates Chk2-dependent G1/S cell cycle arrest. *PloS One* **9**, e87299 (2014).

604 8. T. Sommermann, K. O'Neill, D. R. Plas, E. Cahir-McFarland, IKKβ and NFκB transcription
605 govern lymphoma cell survival through AKT-induced plasma membrane trafficking of
606 GLUT1. *Cancer Res.* **71**, 7291–7300 (2011).

607 9. S. Darekar, *et al.*, Epstein-Barr Virus Immortalization of Human B-Cells Leads to Stabilization
608 of Hypoxia-Induced Factor 1 Alpha, Congruent with the Warburg Effect. *PLoS ONE* **7**
609 (2012).

610 10. L. W. Wang, *et al.*, Epstein-Barr-Virus-Induced One-Carbon Metabolism Drives B Cell
611 Transformation. *Cell Metab.* **30**, 539-555.e11 (2019).

612 11. M. Sola-Penna, Metabolic regulation by lactate. *IUBMB Life* **60**, 605–608 (2008).

613 12. S. Sun, H. Li, J. Chen, Q. Qian, Lactic Acid: No Longer an Inert and End-Product of Glycolysis.
614 *Physiology* **32**, 453–463 (2017).

615 13. J. Chiche, *et al.*, In vivo pH in metabolic-defective Ras-transformed fibroblast tumors: Key role
616 of the monocarboxylate transporter, MCT4, for inducing an alkaline intracellular pH. *Int. J.*
617 *Cancer* **130**, 1511–1520 (2012).

618 14. A. P. Halestrap, N. T. Price, The proton-linked monocarboxylate transporter (MCT) family:
619 structure, function and regulation. *Biochem. J.* **343 Pt 2**, 281–299 (1999).

620 15. A. Ritzhaupt, I. S. Wood, A. Ellis, K. B. Hosie, S. P. Shirazi-Beechey, Identification and
621 characterization of a monocarboxylate transporter (MCT1) in pig and human colon: its
622 potential to transport L-lactate as well as butyrate. *J. Physiol.* **513 (Pt 3)**, 719–732 (1998).

623 16. W. N. Fishbein, N. Merezhinskaya, J. W. Foellmer, Relative distribution of three major lactate
624 transporters in frozen human tissues and their localization in unfixed skeletal muscle.
625 *Muscle Nerve* **26**, 101–112 (2002).

626 17. B. Deuticke, Monocarboxylate transport in erythrocytes. *J. Membr. Biol.* **70**, 89–103 (1982).

627 18. N. T. Price, V. N. Jackson, A. P. Halestrap, Cloning and sequencing of four new mammalian
628 monocarboxylate transporter (MCT) homologues confirms the existence of a transporter
629 family with an ancient past. *Biochem. J.* **329 (Pt 2)**, 321–328 (1998).

630 19. K. S. Dimmer, B. Friedrich, F. Lang, J. W. Deitmer, S. Bröer, The low-affinity monocarboxylate
631 transporter MCT4 is adapted to the export of lactate in highly glycolytic cells. *Biochem. J.*
632 **350 Pt 1**, 219–227 (2000).

633 20. C. S. Hong, *et al.*, MCT1 modulates cancer cell pyruvate export and growth of tumors that co-
634 express MCT1 and MCT4. *Cell Rep.* **14**, 1590–1601 (2016).

635 21. J. R. Doherty, J. L. Cleveland, Targeting lactate metabolism for cancer therapeutics. *J. Clin.*
636 *Invest.* **123**, 3685–3692 (2013).

637 22. J. R. Doherty, *et al.*, Blocking Lactate Export by Inhibiting the Myc Target MCT1 Disables
638 Glycolysis and Glutathione Synthesis. *Cancer Res.* **74**, 908–920 (2014).

639 23. D. M. Voss, *et al.*, Disruption of the monocarboxylate transporter-4-basigin interaction inhibits
640 the hypoxic response, proliferation, and tumor progression. *Sci. Rep.* **7** (2017).

641 24. C. Juel, Lactate-proton cotransport in skeletal muscle. *Physiol. Rev.* **77**, 321–358 (1997).

642 25. A. Bonen, S. K. Baker, H. Hatta, Lactate transport and lactate transporters in skeletal muscle.
643 *Can. J. Appl. Physiol. Rev. Can. Physiol. Appl.* **22**, 531–552 (1997).

644 26. P. D. Bosshart, D. Kalbermatter, S. Bonetti, D. Fotiadis, Mechanistic basis of L-lactate
645 transport in the SLC16 solute carrier family. *Nat. Commun.* **10** (2019).

646 27. S. Hui, *et al.*, Glucose feeds the TCA cycle via circulating lactate. *Nature* **551**, 115–118 (2017).

647 28. D. Whitaker-Menezes, *et al.*, Evidence for a stromal-epithelial “lactate shuttle” in human
648 tumors. *Cell Cycle* **10**, 1772–1783 (2011).

649 29. M. Beloueche-Babari, *et al.*, MCT1 inhibitor AZD3965 increases mitochondrial metabolism,
650 facilitating combination therapy and non-invasive magnetic resonance spectroscopy.
651 *Cancer Res.* **77**, 5913–5924 (2017).

652 30. D. Benjamin, *et al.*, Dual Inhibition of the Lactate Transporters MCT1 and MCT4 Is Synthetic
653 Lethal with Metformin due to NAD+ Depletion in Cancer Cells. *Cell Rep.* **25**, 3047-3058.e4
654 (2018).

655 31. , A Phase I Trial of AZD3965 in Patients With Advanced Cancer - Full Text View -
656 ClinicalTrials.gov (April 14, 2020).

657 32. N. J. Curtis, *et al.*, Pre-clinical pharmacology of AZD3965, a selective inhibitor of MCT1:
658 DLBCL, NHL and Burkitt's lymphoma anti-tumor activity. *Oncotarget* **8**, 69219–69236
659 (2017).

660 33. C. Kaiser, *et al.*, The Proto-Oncogene c-myc Is a Direct Target Gene of Epstein-Barr Virus
661 Nuclear Antigen 2. *J. Virol.* **73**, 4481–4484 (1999).

662 34. A. Pajic, *et al.*, Cell cycle activation by c-myc in a Burkitt lymphoma model cell line. *Int. J.*
663 *Cancer* **87**, 787–793 (2000).

664 35. S. Maier, *et al.*, Cellular Target Genes of Epstein-Barr Virus Nuclear Antigen 2. *J. Virol.* **80**,
665 9761–9771 (2006).

666 36. Ahmad A. Cluntun, Rachit Badolia, Sandra Lettlova, K. Mark Parnell, Thirupura S. Shankar,
667 Nikolaos A. Diakos, Kristofor A. Olson, Iosif Taleb, Jordan A. Berg, Corey N. Cunningham,
668 Alex J. Bott, Aspasia Thodou Krokidi, Sarah Fogarty, Sophia Skedros, Wojciech I. Swiatek,
669 Tyler Van Ry, James E. Cox, Bai Luo, Shannon Merx, Sutip Navankasattusas, Stephen H.
670 McKellar,*, Jared Rutter*, and Stavros G. Drakos*, Mitochondrial Pyruvate Metabolism
671 Modulates Cardiac Hypertrophy and Heart Failure | In Review.

672 37. I. Marchiq, R. Le Floch, D. Roux, M.-P. Simon, J. Pouyssegur, Genetic disruption of lactate/H+
673 symporters (MCTs) and their subunit CD147/BASIGIN sensitizes glycolytic tumor cells to
674 phenformin. *Cancer Res.* **75**, 171–180 (2015).

675 38. M. Bibas, A. Antinori, EBV and HIV-Related Lymphoma. *Mediterr. J. Hematol. Infect. Dis.* **1**
676 (2009).

677 39. S. A. Rezk, L. M. Weiss, Epstein-Barr virus-associated lymphoproliferative disorders. *Hum.*
678 *Pathol.* **38**, 1293–1304 (2007).

679 40. V. R. Dharnidharka, *et al.*, Post-transplant lymphoproliferative disorders. *Nat. Rev. Dis. Primer*
680 **2**, 15088 (2016).

681 41. E. L. Sanchez, *et al.*, Glycolysis, Glutaminolysis, and Fatty Acid Synthesis Are Required for
682 Distinct Stages of Kaposi's Sarcoma-Associated Herpesvirus Lytic Replication. *J. Virol.* **91**
683 (2017).

684 42. M. Lagunoff, Activation of cellular metabolism during latent Kaposi's Sarcoma herpesvirus
685 infection. *Curr. Opin. Virol.* **19**, 45–49 (2016).

686 43. A. P. Bhatt, *et al.*, Dysregulation of fatty acid synthesis and glycolysis in non-Hodgkin
687 lymphoma. *Proc. Natl. Acad. Sci.* **109**, 11818–11823 (2012).

688 44. E. Currie, A. Schulze, R. Zechner, T. C. Walther, R. V. Farese, Cellular fatty acid metabolism
689 and cancer. *Cell Metab.* **18**, 153–161 (2013).

690 45. T. Delgado, *et al.*, Induction of the Warburg effect by Kaposi's sarcoma herpesvirus is required
691 for the maintenance of latently infected endothelial cells. *Proc. Natl. Acad. Sci. U. S. A.*
692 **107**, 10696–10701 (2010).

693 46. M. S. Ullah, A. J. Davies, A. P. Halestrap, The Plasma Membrane Lactate Transporter MCT4,
694 but Not MCT1, Is Up-regulated by Hypoxia through a HIF-1α-dependent Mechanism. *J.*
695 *Biol. Chem.* **281**, 9030–9037 (2006).

696 47. L. Dai, *et al.*, Emmprin and KSHV: New partners in viral cancer pathogenesis. *Cancer Lett.*
697 **337**, 161–166 (2013).

698 48. Z. Qin, L. Dai, M. G. Slomiany, B. P. Toole, C. Parsons, Direct activation of emmprin and
699 associated pathogenesis by an oncogenic herpesvirus. *Cancer Res.* **70**, 3884–3889
700 (2010).

701 49. L. W. Wang, *et al.*, Epstein-Barr virus subverts mevalonate and fatty acid pathways to promote
702 infected B-cell proliferation and survival. *PLoS Pathog.* **15** (2019).

703 50. M. Hulse, *et al.*, Poly(ADP-ribose) polymerase 1 is necessary for coactivating hypoxia-
704 inducible factor-1-dependent gene expression by Epstein-Barr virus latent membrane
705 protein 1. *PLoS Pathog.* **14**, e1007394 (2018).

706 51. J. Xie, *et al.*, Beyond Warburg effect – dual metabolic nature of cancer cells. *Sci. Rep.* **4**
707 (2014).

708 52. H. Wu, M. Ying, X. Hu, Lactic acidosis switches cancer cells from aerobic glycolysis back to
709 dominant oxidative phosphorylation. *Oncotarget* **7**, 40621–40629 (2016).

710 53. W. Ying, NAD+/NADH and NADP+/NADPH in Cellular Functions and Cell Death: Regulation
711 and Biological Consequences. *Antioxid. Redox Signal.* **10**, 179–206 (2007).

712 54. A. A. Khutornenko, *et al.*, Pyrimidine biosynthesis links mitochondrial respiration to the p53
713 pathway. *Proc. Natl. Acad. Sci.* **107**, 12828–12833 (2010).

714 55. S. J. Park, *et al.*, An overview of MCT1 and MCT4 in GBM: small molecule transporters with
715 large implications. *Am. J. Cancer Res.* **8**, 1967–1976 (2018).

716 56. D. Benjamin, *et al.*, Syrosingopine sensitizes cancer cells to killing by metformin. *Sci. Adv.* **2**
717 (2016).

718 57. M. Islas-Ohlmayer, *et al.*, Experimental Infection of NOD/SCID Mice Reconstituted with
719 Human CD34+ Cells with Epstein-Barr Virus. *J. Virol.* **78**, 13891–13900 (2004).

720 58. M. C. Chambers, *et al.*, A cross-platform toolkit for mass spectrometry and proteomics. *Nat.*
721 *Biotechnol.* **30**, 918–920 (2012).

722 59. T. Pluskal, S. Castillo, A. Villar-Briones, M. Orešič, MZmine 2: Modular framework for
723 processing, visualizing, and analyzing mass spectrometry-based molecular profile data.
724 *BMC Bioinformatics* **11**, 395 (2010).

725 60. O. D. Myers, S. J. Sumner, S. Li, S. Barnes, X. Du, One Step Forward for Reducing False
726 Positive and False Negative Compound Identifications from Mass Spectrometry
727 Metabolomics Data: New Algorithms for Constructing Extracted Ion Chromatograms and
728 Detecting Chromatographic Peaks. *Anal. Chem.* **89**, 8696–8703 (2017).

729 61. X. Su, W. Lu, J. D. Rabinowitz, Metabolite Spectral Accuracy on Orbitraps. *Anal. Chem.* **89**,
730 5940–5948 (2017).

731 62. A. M. Price, J. E. Messinger, M. A. Luftig, c-Myc Represses Transcription of Epstein-Barr
732 Virus Latent Membrane Protein 1 Early after Primary B Cell Infection. *J. Virol.* **92**, e01178-
733 17 (2018).

734